UNIVERSITY NAME (IN BLOCK CAPITALS)

Thesis Title

by

Author Name

A thesis submitted in partial fulfillment for the
degree of Doctor of Philosophy

in the

Faculty Name
Department or School Name

March 2018

Declaration of Authorship

I, AUTHOR NAME, declare that this thesis titled, 'THESIS TITLE' and the work presented in it are my own. I confirm that:

- This work was done wholly or mainly while in candidature for a research degree at this University.
- Where any part of this thesis has previously been submitted for a degree or any other qualification at this University or any other institution, this has been clearly stated.
- Where I have consulted the published work of others, this is always clearly attributed.
- Where I have quoted from the work of others, the source is always given. With the exception of such quotations, this thesis is entirely my own work.
- I have acknowledged all main sources of help.
- Where the thesis is based on work done by myself jointly with others, I have made clear exactly what was done by others and what I have contributed myself.

Signed: _____

Date: _____

"Write a funny quote here."

If the quote is taken from someone, their name goes here

UNIVERSITY NAME (IN BLOCK CAPITALS)

Abstract

Faculty Name
Department or School Name

Doctor of Philosophy

by Author Name

The Thesis Abstract is written here (and usually kept to just this page). The page is kept centered vertically so can expand into the blank space above the title too...

Acknowledgements

The acknowledgements and the people to thank go here, don't forget to include your project advisor...

Contents

List of Figures

List of Tables

Abbreviations

LAH **L**ist **A**bbreviations **H**ere

Physical Constants

Speed of Light $c = 2.997\ 924\ 58 \times 10^8\ \mathrm{ms}^{-\mathrm{S}}$ (exact)

Symbols

a	distance	m
P	power	W (Js^{-1})
ω	angular frequency	rads^{-1}

For/Dedicated to/To my...

Chapter 1

Results

Simulations were peformed on system sizes $L = 40, 48, 64, 80, 104, 128$ with the λs taken from zero to one in steps of 0.2 and also 1.5 where λ_x and λ_y had the same magnitude and the same or opposite signs.

1.1 Linear Case

Figure. **??** overlays the Binder cumulant evolution for different sizes in the linear ($\lambda_x = \lambda_y = 0$) case which corresponds to the XY model. Figure. 1.1 does the same but plotted with respect to $t/L^2 \log t$ where the collapse is expected. As is clear, this reobtains the result from [1] while using Stochastic evolution rather than Monte Carlo and provides confidence in the results for the non-linear cases. The collapse is not perfect: Figures 1.2 and 1.3, which display the Binder cumulant as a function of the number of realisations for all the system sizes, show how far apart the curves are. A value of $t/L^2 \log t$ was calculated for $L = 40$ for two points in the simulation, namely, midway through and three quarters of the way thourgh, and the corresponding t was chosen for all other system sizes that was closest to this value. In this report we call these the midway and three quarters graph for brevity. For the first case, the uncertainties of the points do not all cross, although none are isolated. In the second case, the collapse is weaker and $L = 48$ is consistently isolated, as can be seen from the graph of the collapse. This also occurs for $L = 64$ earlier on in the simulation. For $L = 48$ there could be an underestimation of the error, and there is a slight downward decrease in its value as the number of realisations is increased. Ideally one would perform further simulations to ensure this, but this was not possible in the time constraints of the project.

With those caveats in mind, we may be assured that the result has been obtained, and this is further corroborated by the plots of $\log n_v$, where n_v is the number of vortices, as a

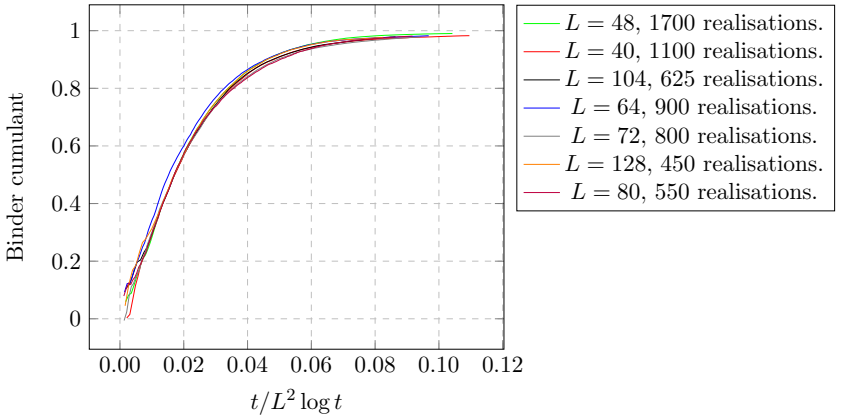

FIGURE 1.1: The Binder cumulant as a function of $t/L^2 \log t$ for different sizes with $\lambda_x = \lambda_y = 0$.

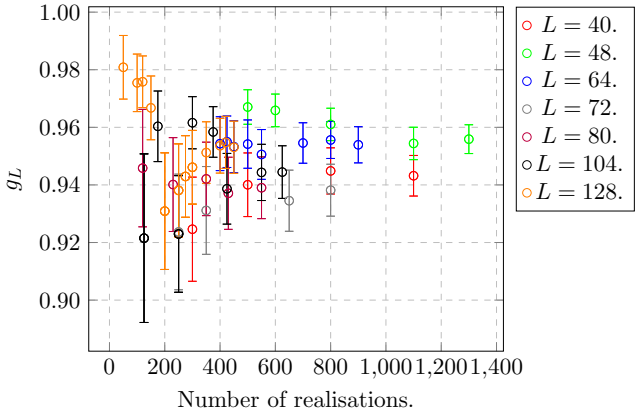

FIGURE 1.2: The uncertainty in the Binder cumulant as a function of the number of realisations at a point closest to $t/L^2 \log t$ for $t = 6500$ (the mid-point of the simulation) for $L = 40.\lambda_x = \lambda_y = 0$.

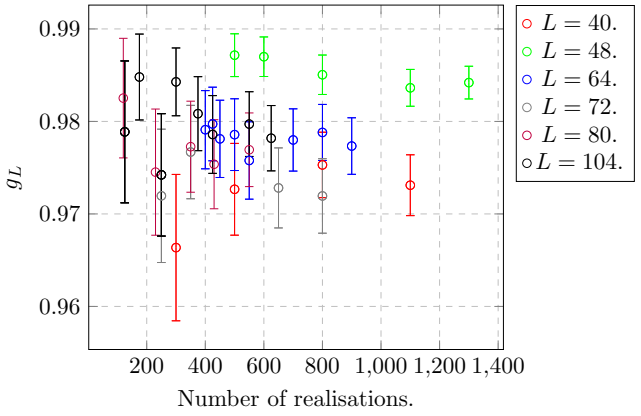

FIGURE 1.3: The uncertainty in the Binder cumulant as a function of the number of realisations at a point closest to $t/L^2 \log t$ for $t = 937.5$ (three quarters through the simualtion) for $L = 40$. $\lambda_x = \lambda_y 0$. There is no value for 128.

function of $\log(t/\log t)$, shown in **??** to1.26 for each system size. For the linear case, it is expected that $\log n_v = -\log(t/\log t)$. This can be explained as follows: using the result in [1] that the distance between vortices R is approximately proportional to $(t/\log t)^{1/2}$, we have that the vortex density is then $1/R^2$, and the number of vortices $n_v \sim L^2/R^2$, and therefore $\log n_v \sim -\log R^2 = -\log(t/\log t)$ up to some additive constants. For brevity, we shall call this the 'vortex gradient.' As the figures show, the gradient was obtained to good accuracy for all system sizes: taking an average for all sizes, we obtain the value -1.001 ± 0.003. Due to the finite size of the system, the approximation breaks down at large times once the majority of the vortices have annihilated, and therefore a time scale must be chosen with which to calculate the gradient. In practice, the time scale maximised but chosen to be prior to the finite size behaviour of the system. Therefore it is sensible not to read the values too literally, but take them as indicative of the behaviour of the linear case.

1.2 Anistropic Case

For non-zero λs, when $\lambda_x = -\lambda_y$, we expect to obtain the same result as the linear case. Figures **??** to **??** show the Binder cumulant plotted as a function of t and also $t/L^2 \log t$ for several values of increasing λ_x. Although the collapse is not as tight as for the linear case, it clearly still occurs to an extent, confirming the expectation. For the case $\lambda_x = 0.2$, the curves do not cross each other as closely as in the linear case at the mid-point of the simulation, however looking at the uncertainties shows that only the $L = 80$ size deviates from the others. All other points are within each other when considering the uncertainties. These conclusions also apply after three quarters of the simulation has completed. This is corroborated by the grandient in vortex gradient which is averaged to be -1.001 ± 0.003, demonstarted linear behaviour.

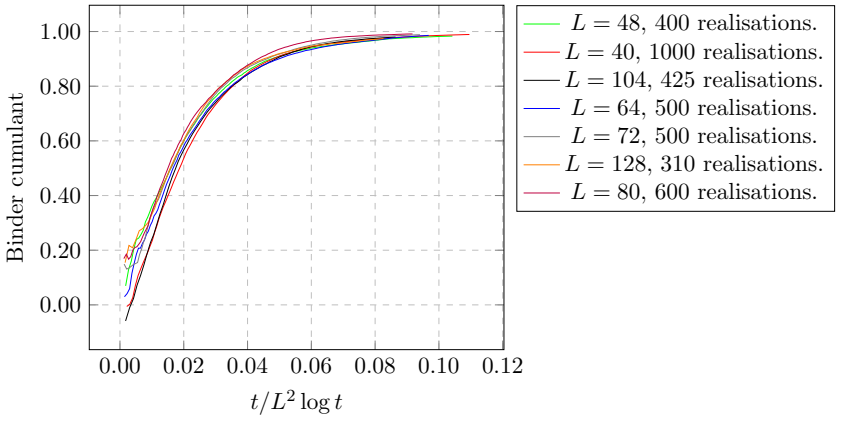

FIGURE 1.4: The Binder cumulant as a function of $t/L^2 \log t$ for different sizes with $\lambda_x = -\lambda_y = 0.2$.

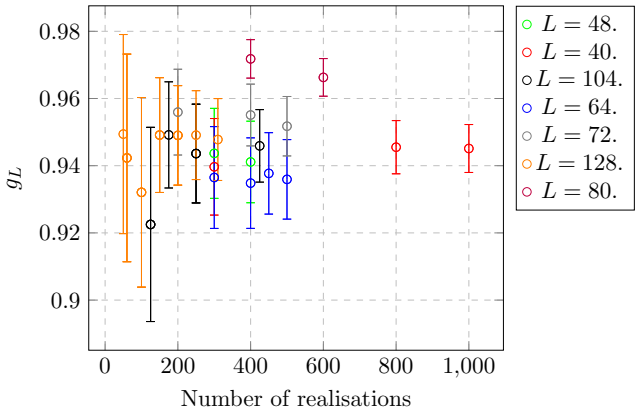

FIGURE 1.5: The uncertainty in the Binder cumulant as a function of the number of realisations at a point closest to $t/L^2 \log t$ for $t = 6500$ (the mid-point of the simulation) for $L = 40.\lambda_x = -\lambda_y = 0.2$.

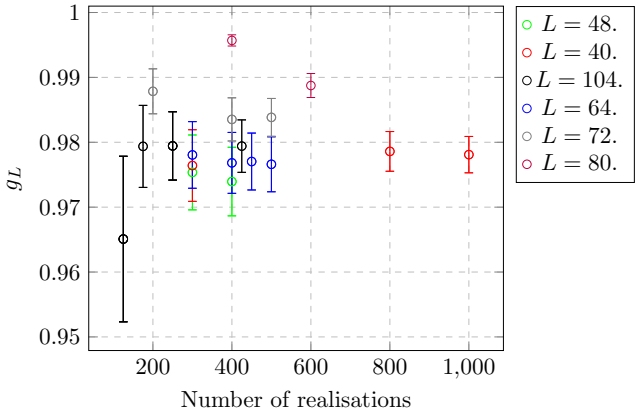

FIGURE 1.6: The uncertainty in the Binder cumulant as a function of the number of realisations at a point closest to $t/L^2 \log t$ for $t = 937.5$ (three quarters through the simualtion) for $L = 40$. $\lambda_x = -\lambda_y = 0.2$. There is no value for 128.

For $\lambda_x = 0.4$ there are similar conclusions to be made. $L = 80$ also deviates, while the mid point uncertainties in the Binder cumulant are within each other for other system sizes. Due to these errors on the Binder cumulant, it would appear that it is undetermined whether further realisations are necessary to tighten the collapse further, or if the dynamical exponent growth rate $(t/\log t)^{1/2}$ is simply not as good an approximation as in the linear case. On the other hand, the vortex gradient does show deviation in its calculated average of -1.013 ± 0.003. As these decrease for higher values of λ monotonically it is clear that the effects of higher values of λ are beginning to be felt. In particular, the convergence of the Binder cumulant becomes faster as λ increases, indicating a faster transition to the ordered phase.

To test how this effects the collapse of the Binder cumulant, we can reverse the process which determined the gradient from the correlation length. Therefore the Binder cumulant should be plotted as a function of $(t/logt)^{\alpha/2}$ where α is the gradient of the vortex plot. Similarly to how [1] plotted the collapse with an effective exponent $z = 2.35$, the

purpose of this plot does not have a physical origin but to demonstrate that the $t/\log t$ must be modified. It should be again noted that [**PhysRevB.94.104520**] only has calculations for the first and second order (in λ) terms for the force between vortices in the weakly isotropic case, where the terms were repulsive at large distances. In the following they appear to be attractive.

For $\lambda_x = 0.4$, the plot of the Binder cumulant as a function of $(t/\log t)^1.013/L^2$ is shown in XX. The collapse is only slightly tighter. The gradient, however, has not significantly deviated from the linear case, so this is not unexpected. In both cases the collapse is still weaker than the linear case. Noting the previous comments on the uncertainties, further simulations are indeed necessary, but there are also are differences to the linear case.

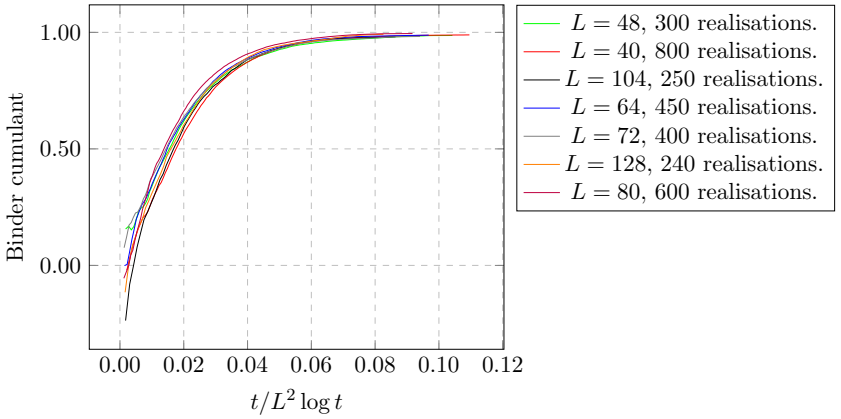

FIGURE 1.7: The Binder cumulant as a function of $t/L^2 \log t$ for different sizes with $\lambda_x = -\lambda_y = 0.4$.

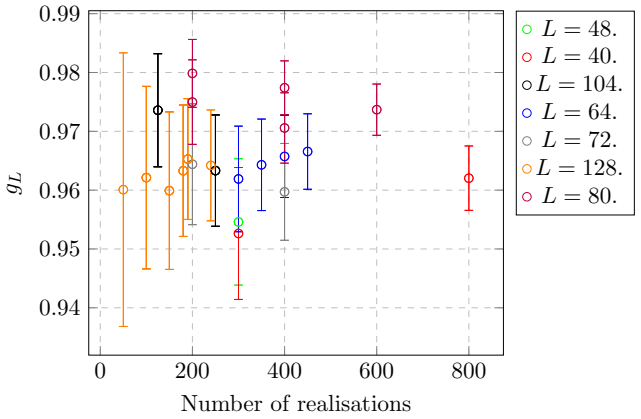

FIGURE 1.8: The uncertainty in the Binder cumulant as a function of the number of realisations at a point closest to $t/L^2 \log t$ for $t = 6500$ (the mid-point of the simulation) for $L = 40.\lambda_x = -\lambda_y = 0.4$.

For the remaining values of λ, we compare both the collapse with an exponent $\alpha = 1$ and one calculated from the gradient. As one increases λ the collapse becomes weaker with a linear exponent but does not appear to degrade in any linear fashion with the

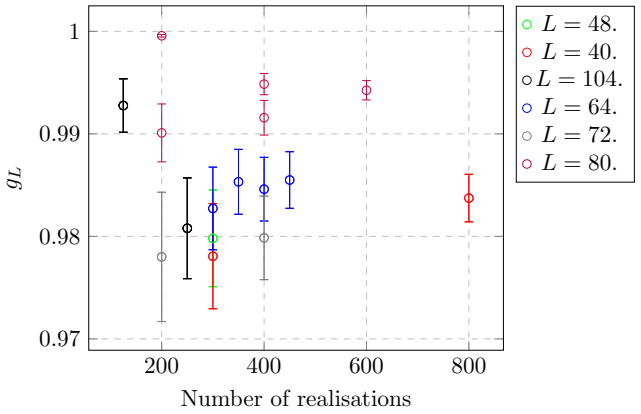

FIGURE 1.9: The uncertainty in the Binder cumulant as a function of the number of realisations at a point closest to $t/L^2 \log t$ for $t = 937.5$ (three quarters through the simualtion) for $L = 40$. $\lambda_x = \lambda_y - 0.4$ There is no value for 128.

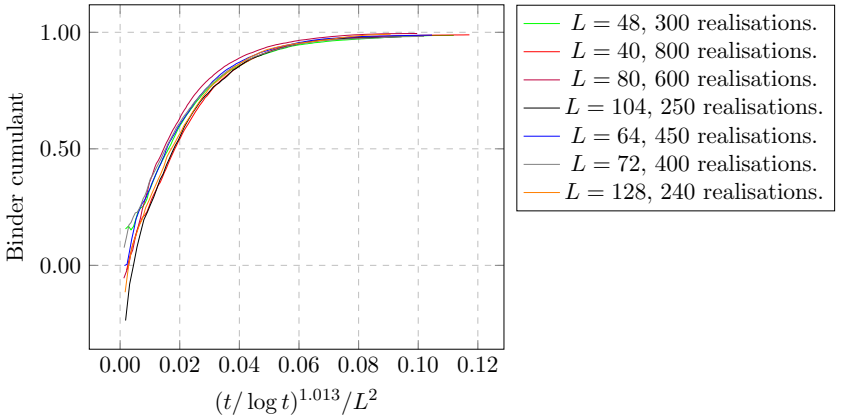

FIGURE 1.10: The Binder cumulant as a function of $(t/\log t)^{1.013}/L^2$ for different sizes with $\lambda_x = -\lambda_y = 0.4$.

modified exponent. In fact, a subjective glance seems to indicate it actually improves, with $\lambda = 1.5$ showing the strongest collapse besides the linear case.

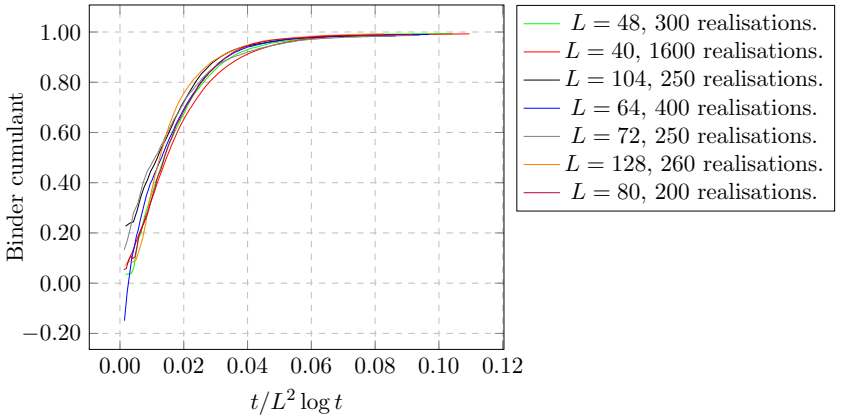

FIGURE 1.11: The Binder cumulant as a function of $t/L^2 \log t$ for different sizes with $\lambda_x = -\lambda_y = 0.6$.

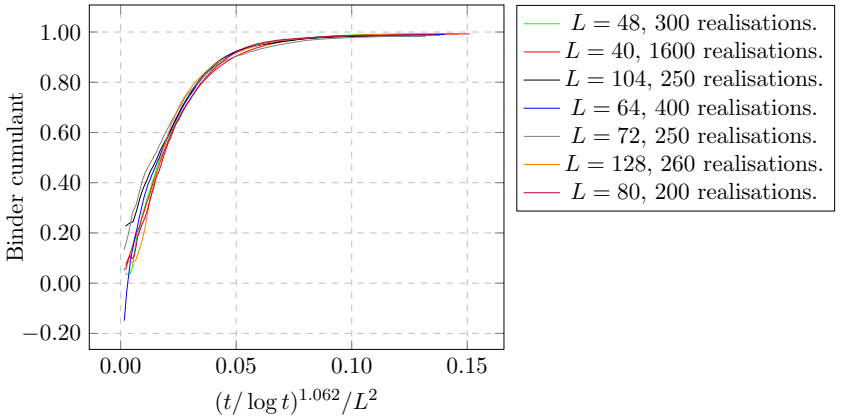

FIGURE 1.12: The Binder cumulant as a function of $(t/\log t)^{1.062}/L^2$ for different sizes with $\lambda_x = -\lambda_y = 0.6$.

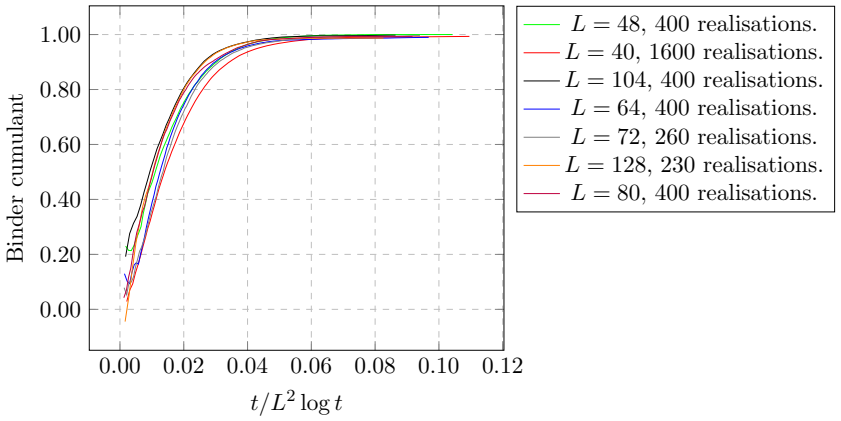

FIGURE 1.13: The Binder cumulant as a function of $t/L^2 \log t$ for different sizes with $\lambda_x = -\lambda_y = 0.8$.

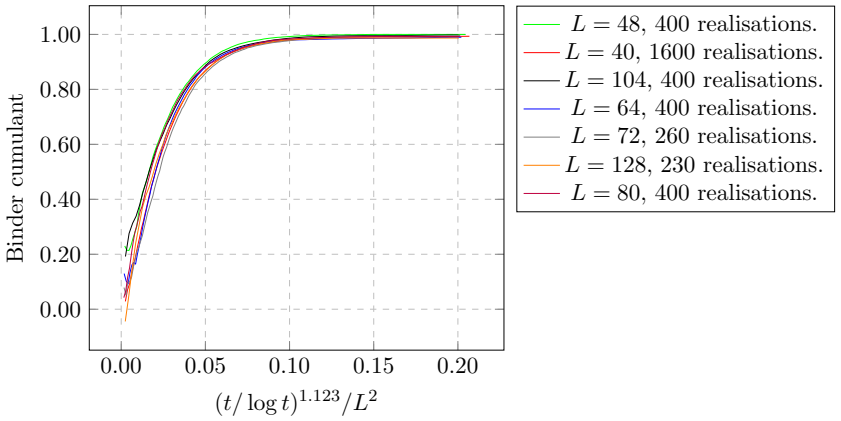

FIGURE 1.14: The Binder cumulant as a function of $(t/\log t)^{1.123}/L^2$ for different sizes with $\lambda_x = -\lambda_y = 0.8$.

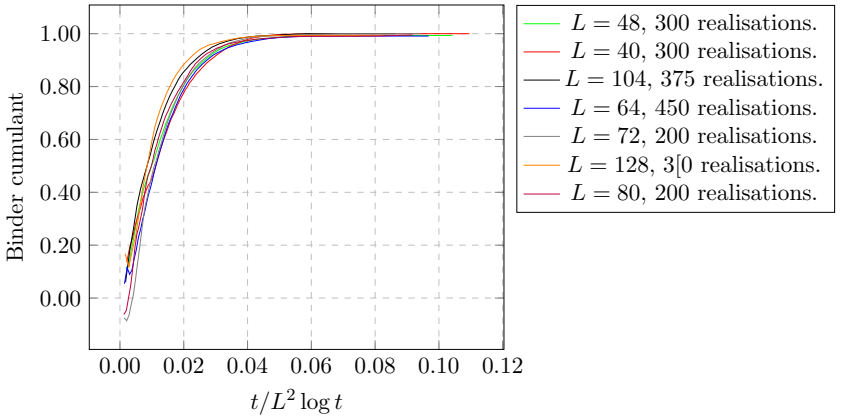

FIGURE 1.15: The Binder cumulant as a function of $t/L^2 \log t$ for different sizes with $\lambda_x = -\lambda_y = 1$.

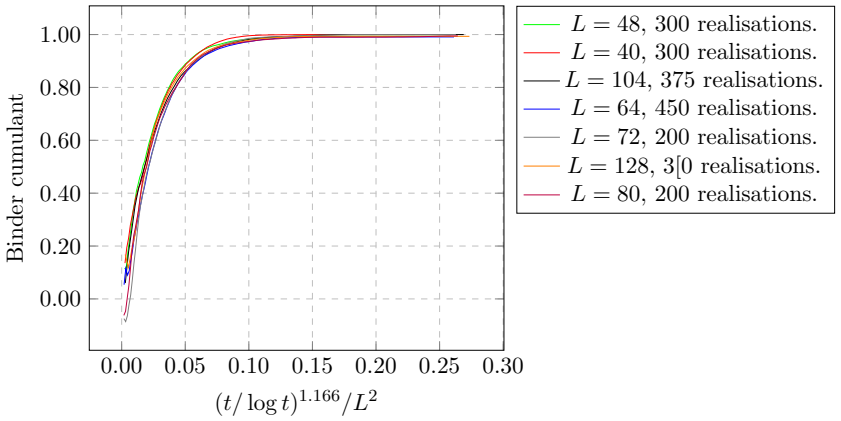

FIGURE 1.16: The Binder cumulant as a function of $(t/\log t)^{1.166}/L^2$ for different sizes with $\lambda_x = -\lambda_y = 1$.

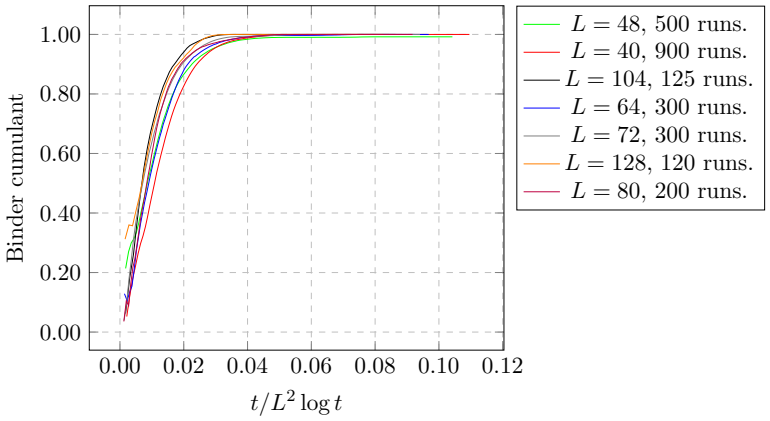

FIGURE 1.17: The Binder cumulant as a function of $t/L^2 \log t$ for different sizes with $\lambda_x = -\lambda_y = 1.5$.

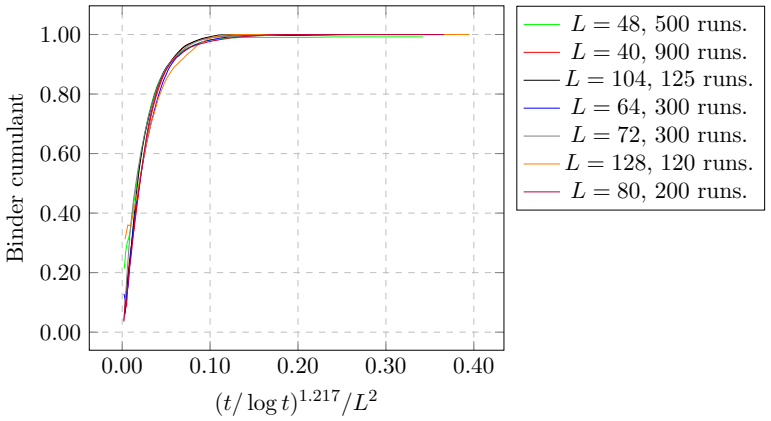

FIGURE 1.18: The Binder cumulant as a function of $(t/\log t)^{1.217}$ for different sizes with $\lambda_x = -\lambda_y = 1.5$.

To check if this is perhaps a finite size effect, although there is no immediate indication that this should be the case, with the calculations in [**PhysRevX.7.041006**] showing that spatial correlations are algebraic as in the XY model below the BKT transitions, the gradient was check for system sizes of $L = 512$. This was for $\mathrm{d}t = 0.05$ and a much lower number of realisations, so not directly comparable, but at least the behaviour of decreasing gradient with increasing λ also follows. Further study into these areas is clearly necessary.

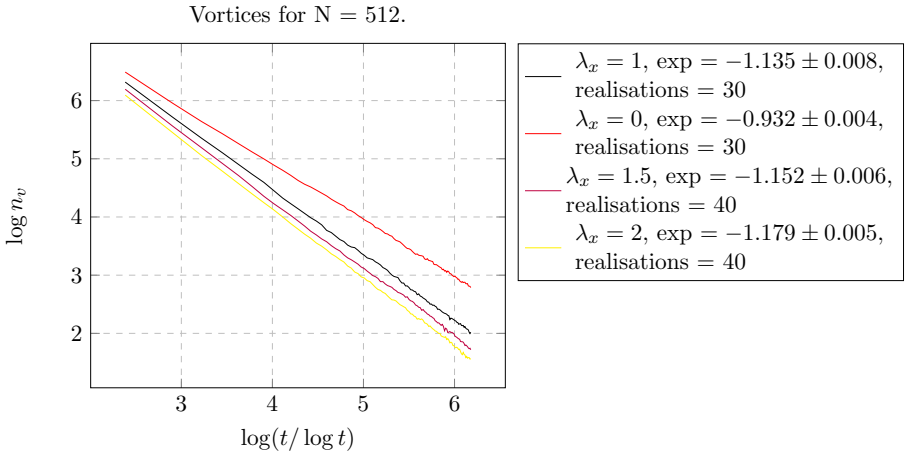

FIGURE 1.19: Log of the number of vortices as a function of $\log(t/\log t)$ for $L = 512$ in the anistropic case.

1.3 Isotrpic case

In the isotropic case, due to the non-linearity, we expect a repulsive contribution of the vortex force at large calculated in [**PhysRevB.94.104520**] with the second order

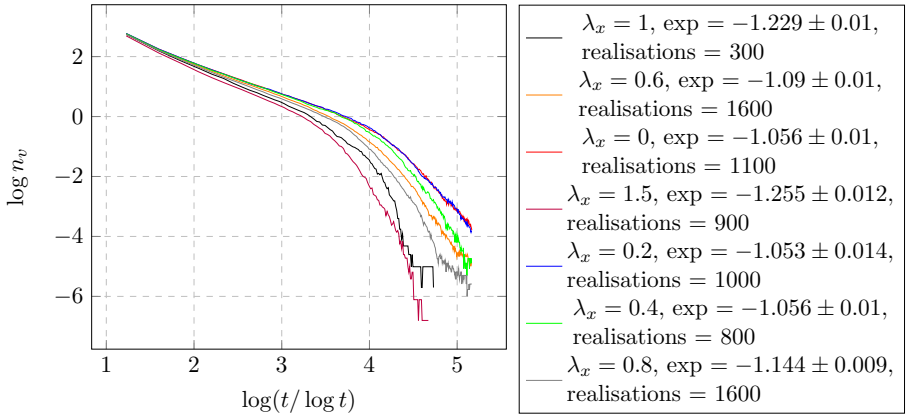

FIGURE 1.20: Log of the number of vortices as a function of $\log(t/\log t)$ for $L = 40$ in the anistropic case.

??

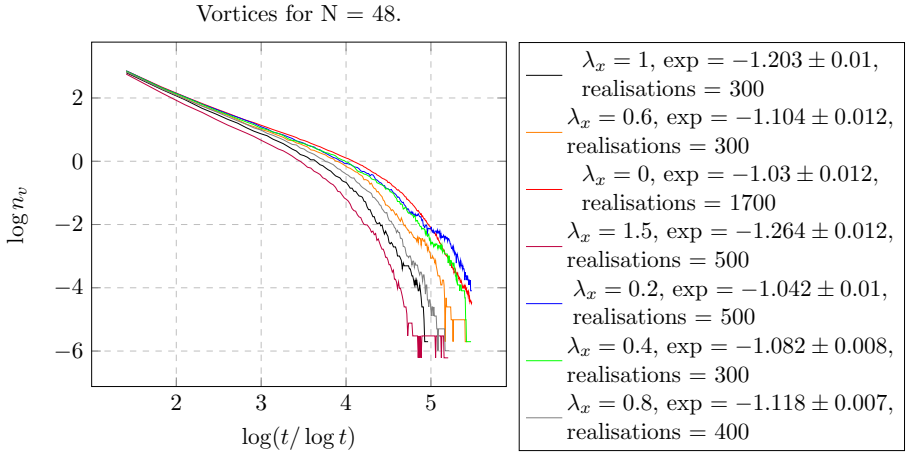

FIGURE 1.21: Log of the number of vortices as a function of $\log(t/\log t)$ for $L = 48$ in the anistropic case.

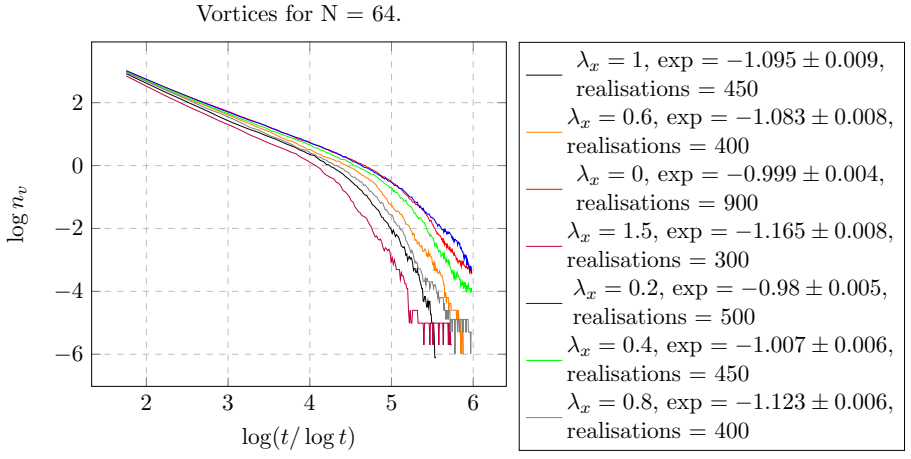

FIGURE 1.22: Log of the number of vortices as a function of $\log(t/\log t)$ for $L = 64$ in the anistropic case.

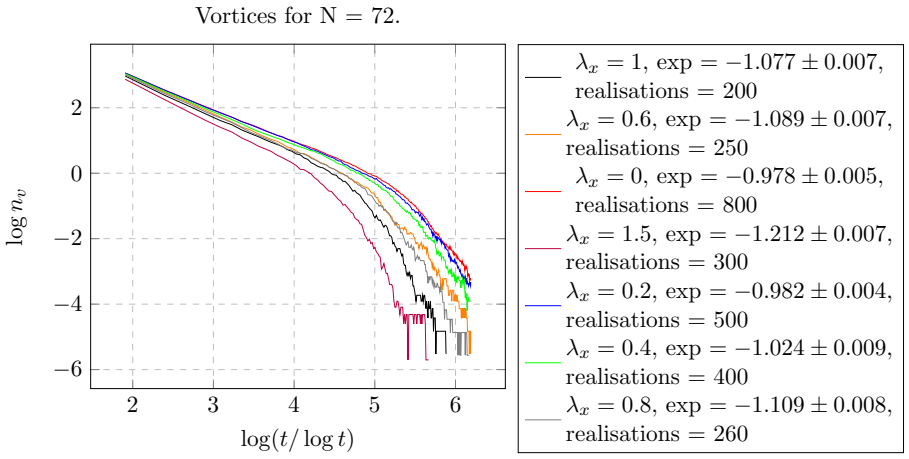

FIGURE 1.23: Log of the number of vortices as a function of $\log(t/\log t)$ for $L = 72$ in the anistropic case.

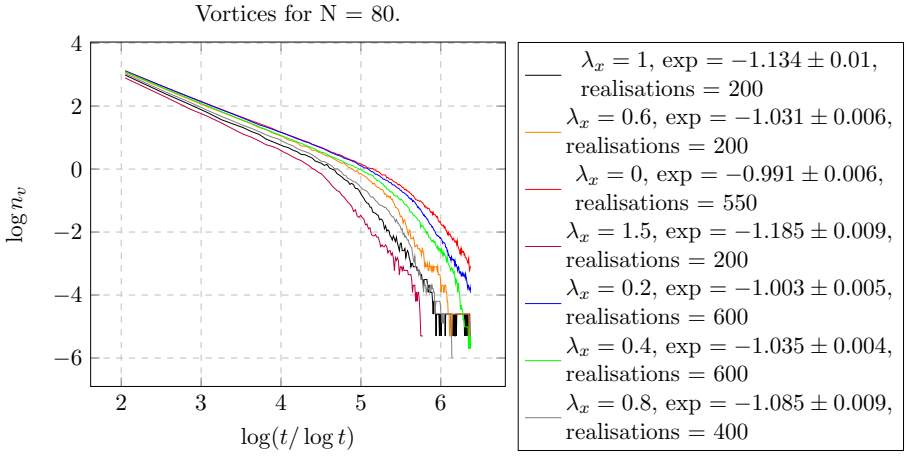

FIGURE 1.24: Log of the number of vortices as a function of $\log(t/\log t)$ for $L = 80$ in the anistropic case.

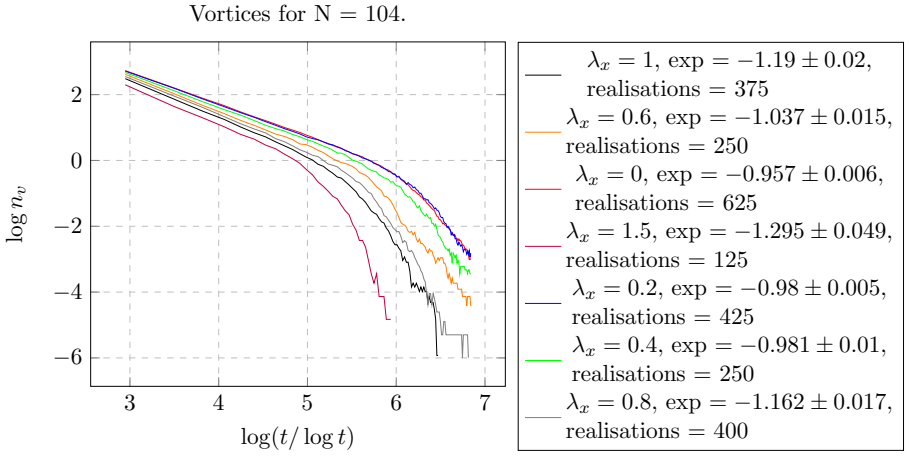

FIGURE 1.25: Log of the number of vortices as a function of $\log(t/\log t)$ for $L = 104$ in the anistropic case.

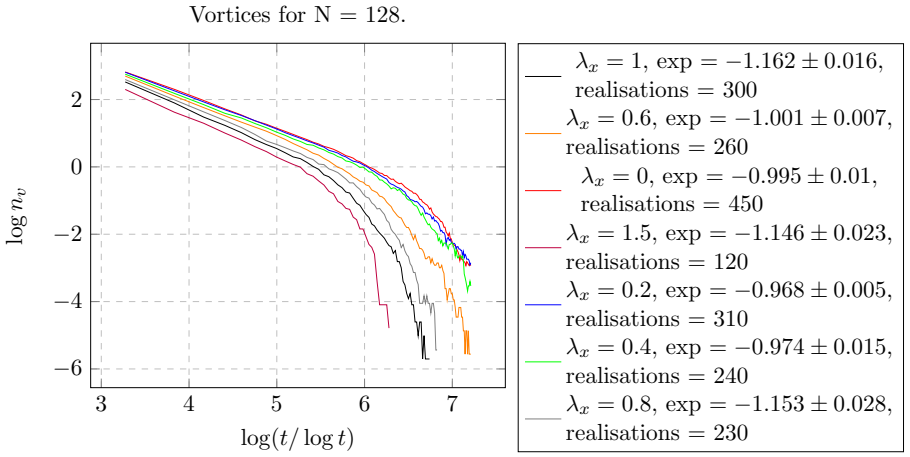

FIGURE 1.26: Log of the number of vortices as a function of $\log(t/\log t)$ for $L = 128$ in the anistropic case.

result, the first order being a force perpendicular to the line joining the vortices, of

$$\boldsymbol{f}(\boldsymbol{R}) = \frac{1}{8}\left(\frac{\lambda}{2D}\right)^2 + \frac{1}{\epsilon}\frac{\boldsymbol{R}}{R^2}(8\log(R/a)^2 + 4\log(R/a) - 1)$$

where R is the vortex separation, ϵ the dielectric constant, and a the lattice spacing. Thus, beyond a certain length scale vortex unbinding should occur–the vortex dominated phase–although this is not the same as the entropic unbinding in the XY case, estimated from equlibrium thermodynamics. Also in the paper the estimate for distance at which this correction term dominates and is given by

$$L_v = ae^{\frac{2D}{\lambda}}.$$

These conclusions are matched by the results. Figure. **??** shows the collapse for $\lambda_x = 0.2$ and the quality is comparable to the anisotropic case. This is as anticipated as we do not expect drastic change in the qualitative behaviour away from a critical point, and provides further confidence in the obtained results. Although the points in the uncertainty graph appear to all cross each other when including the errors, the uncertainties are much larger. The average vortex gradient is -0.953 ± 0.005, so has already altered unlike in the anisotropic case. This is in the direction we expect, where the the vortex recombination occurs at a slower rate due to their reduced attractions. In brief, the behaviour is slighty but not significantly different from the linear case.

Figures XX and XX show the uncertainties for $\lambda_x = 0.2$.

The case $\lambda_x = 0.4$ is more interesting, where the efefcts of the non-linearity are much more pronounced. This provides a clear demonstration of the expectation in that the 'destruction' of the convergence of the Binder cumulant occurs first for the largest system

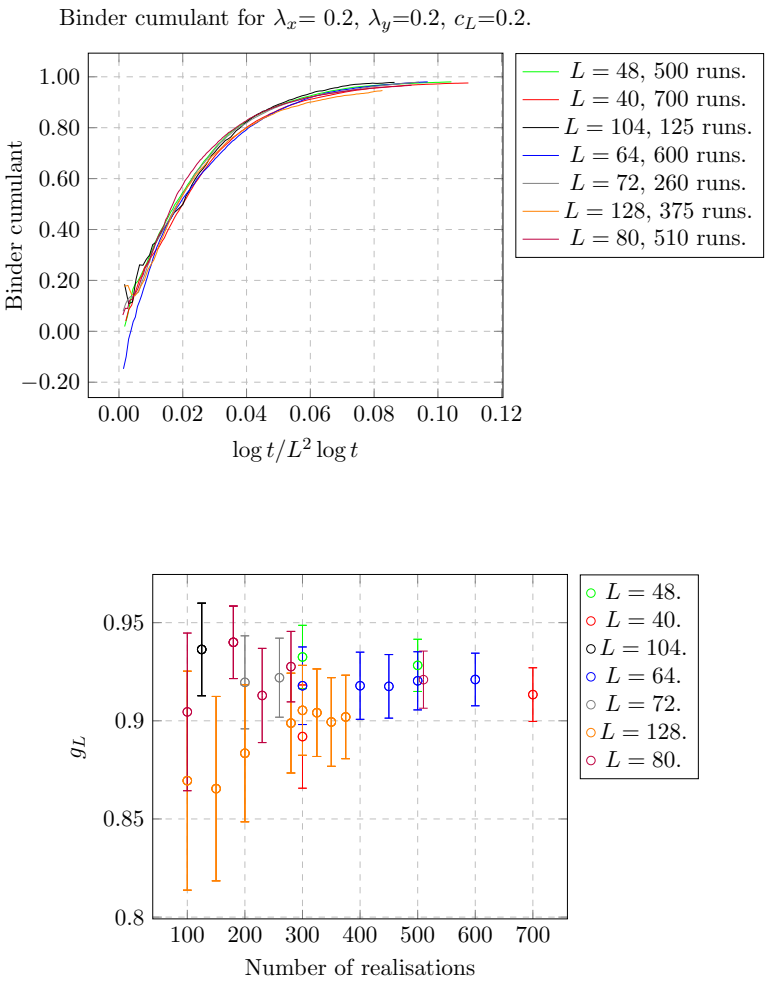

FIGURE 1.27: The uncertainty in the Binder cumulant as a function of the number of realisations at a point closest to $t/L^2 \log t$ for $t = 6500$ (the mid-point of the simulation) for $L = 40.\lambda_x = \lambda_y = 0.2$.

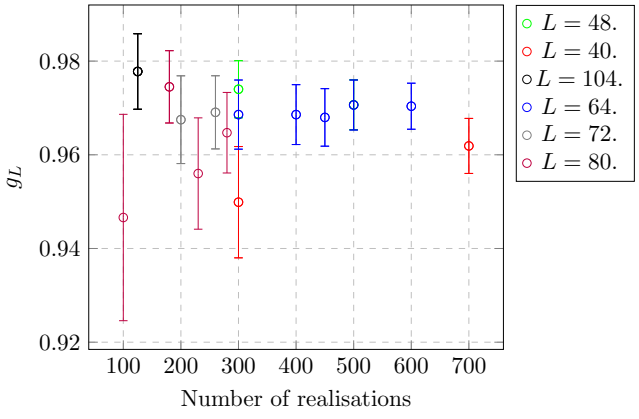

FIGURE 1.28: The uncertainty in the Binder cumulant as a function of the number of realisations at a point closest to $t/L^2 \log t$ for $t = 9370$ (the mid-point of the simulation) for $L = 40.\lambda_x = \lambda_y = 0.2$.

and gradually lessens for the smaller system as can be seen from the order of the curves in the plot. There is also a weak pattern in the increase of the vortex gradient as the system size is increased, ranging from -0.928 ± 0.015 for $L = 40$ to -0.807 ± 0.009 for $L = 128$, whereas no such pattern occurs in the linear case.

As for the uncertainties, they are all larger and in general the points are not overlapping, although this can be seen from the graph of the Binder cumulant. The uncertainty in the sizes $L = 104$ and $L = 128$ are much larger, and the for these sizes the Binder cumulant is fluctuating.

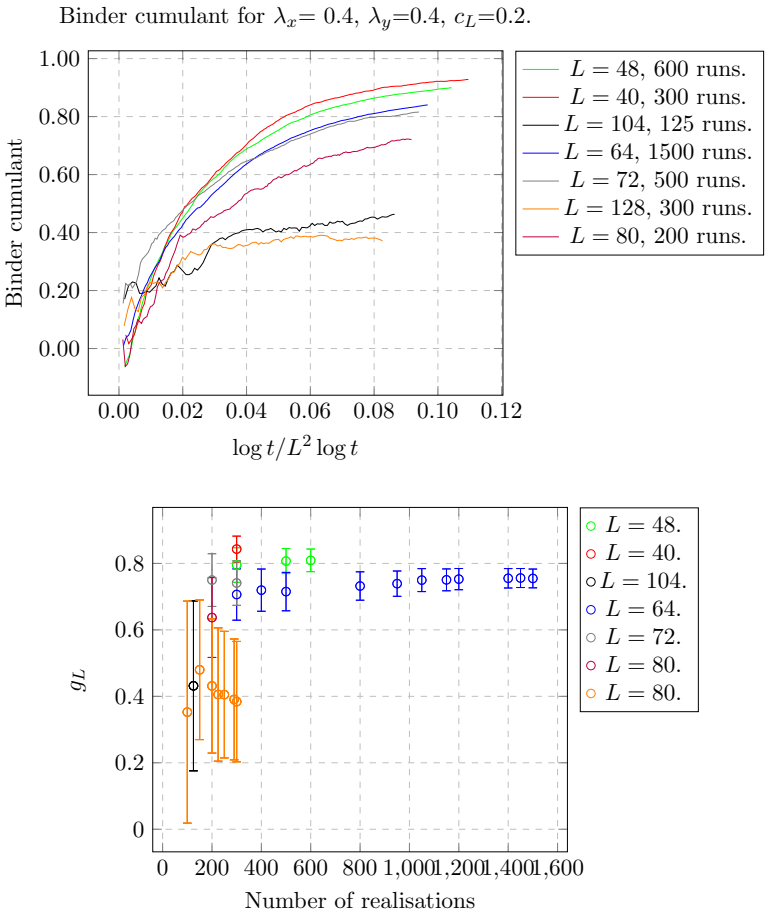

FIGURE 1.29: The uncertainty in the Binder cumulant as a function of the number of realisations at a point closest to $t/L^2 \log t$ for $t = 650$ (three quarters through the simualtion) for $L = 40$. $\lambda_x = \lambda_y = 0.4$.

By observing the behaviour of the Binder cumulant as λ is increased further, a clear pattern emerges.

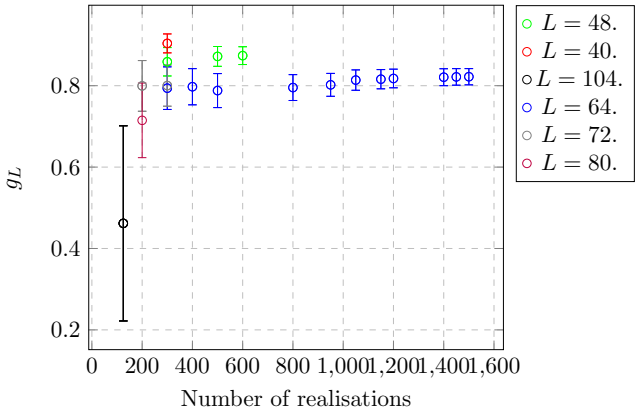

FIGURE 1.30: The uncertainty in the Binder cumulant as a function of the number of realisations at a point closest to $t/L^2 \log t$ for $t = 937.5$ (three quarters through the simualtion) for $L = 40$. $\lambda_x = \lambda_y = 0.4$. There is no value for 128.

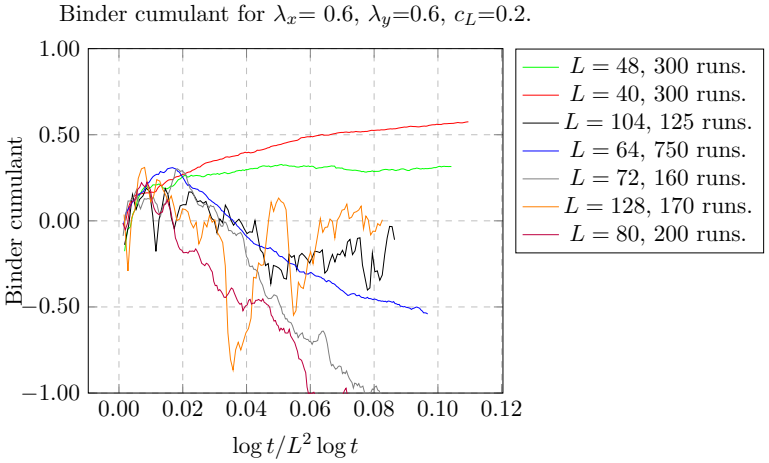

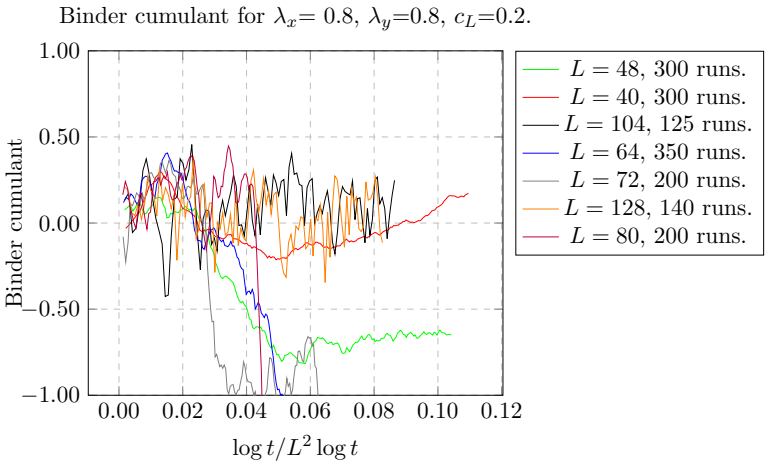

Binder cumulant for λ_x= 1, λ_y=1, c_L=0.2.

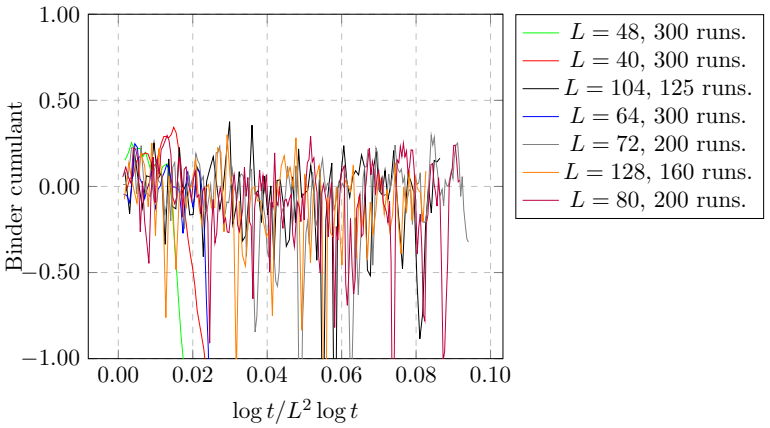

Binder cumulant for λ_x= 1.5, λ_y=1.5, c_L=0.2.